IET Nanobiotechnology

Special Issue: Selected extended papers from the 2nd International Conference on Nanoscience and Nanotechnology (ICNAN2019)

Fabrication and characterization of biodegradable PHBV/SiO_2 nanocomposite for thermo-mechanical and antibacterial applications in food packaging

ISSN 1751-8741
Received on 28th February 2020
Revised 22nd May 2020
Accepted on 2nd June 2020
E-First on 15th September 2020
doi: 10.1049/iet-nbt.2020.0066
www.ietdl.org

Nupur Ojha[1], Nilanjana Das[1] ✉

[1]*Bioremediation Laboratory, Department of Biomedical Sciences, School of Bio Sciences and Technology, Vellore Institute of Technology, Vellore-632014, Tamil Nadu, India*

✉ *E-mail: nilanjanamitra@vit.ac.in*

Abstract: In the present study, biogenic silica nanoparticles (bSNPs) were synthesized from groundnut shells, and thoroughly characterized to understand its phase, and microstructure properties. The biopolymer was synthesized from yeast *Wickerhamomyces anomalus* and identified as Poly (3-hydroxybutyrate-*co*-3-hydroxyvalerate) (PHBV) by GC-MS and NMR analysis. The bSNPs were reinforced to fabricate PHBV/SiO_2 nanocomposites via solution casting technique. The fabricated PHBV/SiO_2 nanocomposites revealed intercalated hybrid interaction between the bSNPs and PHBV matrix through XRD analysis. PHBV/SiO_2 nanocomposites showed significant improvement in physical, chemical, thermo-mechanical and biodegradation properties as compared to the bare PHBV. The cell viability study revealed excellent biocompatibility against L929 mouse fibroblast cells. The antibacterial activity of PHBV/SiO_2 nanocomposites was found to be progressively improved upon increasing bSNPs concentration against *E. coli* and *S. aureus*.

1 Introduction

The most significant role of food packaging materials is to maintain the quality and safety of food products during its transportation and preservation. Also in extending its shelf-life by preventing unfavourable conditions such as chemical contaminants, oxygen, moisture, light, and spoilage from microorganisms [1]. A proper food packaging material should prevent microbial contamination, hinder gain or loss of moisture, act as a barrier against permeation of water vapour, carbon dioxide, oxygen and other volatile compounds. It should have high mechanical strength, excellent thermal, chemical and dimensional stability, recyclability and biodegradability [2]. Over the decades, many synthetic polymers fabricated from non-renewable fossil fuels viz. polyvinylchloride (PVC), polypropylene (PP.), polyethylene terephthalate (PET), polyethylene (PE), polyamide (PA) and polystyrene (PS) have been widely used as food packaging materials due to its broad availability at relatively low cost, excellent mechanical performance such as tensile and impact strength, good barrier properties and heat sealability [3]. However, it needs to be restricted since these synthetic polymers are non-biodegradable and non-recyclable in nature, which causes severe environmental problems.

Consequently, the industry sectors and research scientists are focusing their attention on the development of biodegradable and bio-based materials for sustainable food packaging applications. These biodegradable polymers are mainly classified into three categories which include (i) polymers that are chemically and conventionally synthesized from agro resources, such as, the polylactic acid (PLA) (ii) agro-polymers extracted from biomass, such as plasticised cellulose, starch (thermoplastic starches), proteins, and chitin and (iii) the polymers synthesized by microorganisms, e.g. family of polyhydroxyalkanoates (PHA) [4]. Among all the classes of biodegradable polymers, the most familiar representative used for food packaging are poly(3-hydroxybutyrate) (PHB) and poly(3-hydroxybutyrate-*co*-3-hydroxyvalerate) (PHBV) because of its inherent properties like eco-friendly, biodegradability and biocompatibility [5]. However, naturally produced PHB polymers have limited applications due to their brittle and hydrophobic nature [6]. Incorporation of several monomers for the synthesis of 3-hydroxybutyrate based copolymers were developed to improve the material properties of the PHB polymer. PHBV has been considered as an attractive copolymer because of the ability of many wild-type strains to stably supply precursor for copolymer synthesis and the improved physical properties of the polymer, compared to PHB [7]. Despite its promising commercial potentiality, the significant drawbacks concerning the traditional plastic frequently used in the food packaging field are low heat deflection temperatures, narrow processing window, hydrophilicity, poor barrier performance [4], and low mechanical and structural properties.

Therefore, to overcome these shortcomings, nanomaterials or nanostructure materials which exhibit different dimensions for its structural elements, clusters such as zero dimensions (nanoparticles, nanoclusters etc), one dimension (nanorods and nanotubes), two dimensions (nano-thin films), and three dimensions (nanomaterials) in the range of 1–100 nm [8] were incorporated into polymers. Nano-reinforced PHBV nanocomposites would be a new approach to improve the mechanical and structural properties of the PHBV, thereby extending its applications in fragile environments. Combining nanostructured materials with PHBV can result relatively in a more extensive particle size material (>100 nm), leading to the formation of PHBV nanocomposite [9]. These nanomaterials are having high surface volume ratio exhibit unique physicochemical characteristics, such as solubility, toxicity, strength, magnetism, diffusivity, optics, colour, and thermodynamics [10]. There are reports on PHA nanocomposites using nanofillers such as multi-walled carbon nanotubes (MWCNTs) [11], organophilic montmorillonite (OMMT) [12], silylated kaolinite, bioactive glass, cellulose nanocrystals, layered double hydroxides and cobalt-aluminium layered double hydroxides [13, 14] but these are commercially not cost-effective. Recently, silicon-based nanomaterials such as nanoclay, silica nanoparticles and polyhedral oligomeric silsesquioxanes (POSS) are well known for their reinforcement effect upon the formation of polymeric nanocomposites (NCs) [15].

Therefore, the present work is focused on the synthesis of biogenic silica dioxide (SiO_2) nanoparticles (bSNPs) which were

used to reinforce into PHBV polymer to fabricate PHBV/SiO_2 nanocomposite bearing low cost, biocompatibility. The bSNPs can be employed as unique filler material to improve the performance of the resulting PHBV by enhancing interactions between nanoparticles and PHBV matrix [15]. Besides, the incorporation of active agents (e.g. antimicrobial, antioxidant, oxygen-scavenging) [16] may result in the development of a cost-effective method to control microbial growth and preserve the desirable quality. To the best of our knowledge, no previous work is reported dealing with the fabrication and characterization of bSNPs-reinforced PHBV nanocomposite to improve its thermal, mechanical, barrier, biodegradable, biocompatible and antibacterial properties to meet the requirements in food packaging, which is the primary goal of the current study.

2 Materials and methods

2.1 Production and identification of extracted biopolymer

The yeast strain *Wickerhamomyces anomalus* VIT-NN01 (*W. anomalus*) was used for the synthesis of PHBV as the strain was reported as potential PHBV producer in our previous study [17]. Production medium used for PHBV synthesis was modified mineral salts medium (MSM) contained (g/L) K_2HPO_4 (3.0), Na_2HPO_4 (6.0), corn steep liquor (2.0), NaCl (5.0), $MgSO_4$ (1.0), $CaCl_2$ (0.1) and $FeCl_3$ (0.06) supplemented with 3.5 g sugarcane molasses, 0.5 and 0.5% palm oil [17]. The yeast strain was inoculated in MSM broth with initial pH 8 and incubated at 37°C under shaking condition (120 rpm) for 96 h. The extraction and purification of the polymer were done following the standard protocol as reported in the previous study [17]. The identification of the purified PHBV was done using Gas chromatography-mass spectrophotometric (GC–MS) and Nuclear magnetic resonance (NMR) spectroscopic analysis followed by the standard protocol as demonstrated by Huang *et al.* [18], and Ojha and Das [17].

2.2 Synthesis of biogenic silica nanoparticles (bSNPs)

For the synthesis of bSNPs, groundnut shells were collected from the agricultural field near to Vellore, Tamil Nadu and ground for further use. Dried ground groundnut shells (GS) powder was acid pre-treated to partially hydrolyze the organic substances present in it. For acid hydrolysis, 250 grams of powdered GS was mixed with 500 ml of 1 N HCl using magnetic stirrer and boiled at 100°C for 2 h. The acid-pre-treated GS was washed with Milli-Q water to remove the hydrochloric acid. The residue was dried and further incinerated at 700°C for 2 h using a muffle furnace [19]. The incinerated ash also contains other metals including the silica. For extraction of silica, 100 g of incinerated ash was mixed with 250 ml of 2.5 N NaOH and boiled at 90°C with continuous stirring for 3 h and filtered [20]. The silica was digested from the prepared ash through the following reaction (1):

$$SiO_2 + 2NaOH \rightarrow Na_2SiO_3 + H_2O \quad (1)$$

Then the filtrate of sodium silicate (Na_2SiO_3) was adjusted to pH 7.4 using 20% sulphuric acid (H_2SO_4) under vigorous stirring at room temperature. This reaction of Na_2SiO_3 with H_2SO_4 precipitated the silica by the following reaction (2):

$$Na_2SiO_3 + H_2SO_4 \rightarrow SiO_2 + Na_2SO_4 + H_2O \quad (2)$$

Later, the filtered solution was shaken (100 rpm) at room temperature for 24 h and aged for 48 h. Finally, the precipitated silica was filtered, washed 2–3 times with distilled water to remove sodium sulphate (Na_2SO_4) and dried. Further the extracted dried silica powder was carried out for sintering process to remove the moisture by heating it at 900°C for 2 h under atmospheric condition [20]. The sintered powder of bSNPs was calculated by a conventional gravitational method and further characterized.

2.3 Fabrication of biogenic PHBV/SiO_2 nanocomposites

The purified extracted PHBV was dried in an oven at 60°C for 20 h before use. The synthesized bSNPs were dehydrated at 200°C for 8 h under vacuum to remove physisorbed water for further use. The solution casting technique was used to prepare PHBV films. Fabrication of PHBV and PHBV/SiO_2 nanocomposites was done by combining ultrasonication with the solution casting method to improve the nanofiller dispersion within the matrix. Firstly, a certain amount of bSNPs were dispersed in chloroform by ultrasonication at 100 W for 30 min. Subsequently, the extracted PHBV powder was dissolved at 50°C in the nanoparticle dispersion, and the mixture was sonicated again at 20 W for 20 min [21]. The resulted blend was poured into a glass petri dish to evaporate the chloroform at room temperature and finally dried under vacuum for 48 h to remove the residual solvent. Different concentrations (wt %) of bSNPs ranging from 0.5, 1.0, 1.5 and 2.0 wt % were incorporated to formulate PHBV/SiO_2 nanocomposites.

2.4 Characterization

The characterization of bSNPs, PHBV and PHBV nanocomposites were done using Fourier transform infrared (FT-IR), X-ray diffraction (XRD), Scanning electron microscopy (SEM), Energy-dispersive X-ray spectroscopy (EDX), Thermogravimetric (TG) and Differential scanning calorimetry (DSC) analysis.

Transmission electron microscopy (TEM) (JEOL 2100 HRTEM) was done only for bSNPs to determine its size. The surface morphology and elemental composition of the samples were examined using SEM (FEI Sirion, Eindhoven, Netherlands) coupled with EDX at an accelerating voltage of 200 kV. The samples were fixed with 2.5% glutaraldehyde in 0.05 M cacodylate buffer for 1 h 30 min at 4°C. The dried samples were coated with a gold layer (Edwards S150B) and examined under the SEM [19]. FT-IR analysis was done to determine the functional groups present in the samples. The samples were ground with potassium bromide (KBr) to prepare pellets for FT-IR analysis using FT-IR spectrophotometer (Shimadzu, DR-800) [22]. The crystalline nature of the samples were investigated using XRD analysis (Bruker D8 Advance diffractometer) following the standard protocol [23]. TG and DSC analysis were performed to find out the thermal stability, degradation pattern, crystallization and melting temperature of the PHBV/SiO_2 nanocomposites. Samples (∼12 mg) were melted at 190°C and kept at this temperature for 5 min. Subsequently, cooled to 25°C and reheated to 190°C. The analysis was done (SDTQ600V20.9 Build 20) at the heating rate of 20°C/min in a nitrogen atmosphere [24]. The transition temperatures were taken as the peak maximum or minimum in the DSC curves.

The mechanical properties were determine by tensile strength, Young's modulus and impact strength. Tensile tests were carried out following the standard protocol of ASTM D 638-03 [25] using a servo-hydraulic testing machine (Tinius, H5KS) with a crosshead speed of 1 mm/min and a load cell of 100 kN. Charpy notched impact strength tests were conducted following the ASTM D 6110-10 [26], standard on a CEAST Fractovis dart impact tester using a hammer mass that collided with an energy of 7.10 J on notched specimen bars. All the as per the [26] and the data were collected at 23°C and 50% relative humidity (RH). Three specimens for each PHBV and PHBV/SiO_2 films were tested.

To analyse the water absorption capacity, the samples were dried in a desiccator at 0% relative humidity (RH) for one week. Subsequently, placed in a desiccator at 100% RH and allowed to absorb water until a constant weight was attained. Water uptake capacity (%) was calculated using (3) [27]

$$\text{Water uptake capacity}(\%) = \frac{W_f - W_i}{W_i} \times 100 \quad (3)$$

where, W_i and W_f are the initial and final (equilibrium) weight of the nanocomposites films, respectively. Three replicates for each sample were measured, and the average value was reported.

2.5 Biocompatibility and antibacterial properties

The *in vitro* biocompatibility of the nanocomposites films were evaluated using of L929 mouse fibroblast cell line by MTT assay. For this study, the PHBV/SiO_2 films having different SiO_2 content (0.5, 1.0, 1.5 and 2.0 wt. %) were cut into discs and sterilized using 70% ethanol and UV treatment. The L929 mouse fibroblast cells cultured in DMEM (Dulbecco's modified eagle medium) supplemented with 10% fetal bovine serum and 1X antibiotic antimycotic solution (Himedia, India). The cells were seeded onto the PHBV/SiO_2 films at concentrations of 1×10^5 cells/well in a 96 well plate and incubated at 37°C for 24, 48 and 72 h to get attached to the films. To the cultured cells, fresh medium containing MTT (0.5 mg/mL) was added and incubated for 3 h at 37°C in a humidified atmosphere containing 5% CO_2. The MTT solution was removed, and the formazan crystals formed were dissolved with DMSO and incubated in dark conditions for 1 h. The absorbance of the solution was measured at 570 nm [28] using a 96-well plate reader (Bio-Rad, CA, USA). All experiments were done in triplicates. Data were collected for triplicates of each nanocomposites, and these data were used to calculate the mean. The percent inhibition was calculated from these data using (4)

$$\text{Cell viability}\,\% = \frac{\text{OD}_\text{c} - \text{OD}_\text{t}}{\text{OD}_\text{c}} \times 100 \tag{4}$$

where OD_c and OD_t are the mean value of the optical density of untreated cells (control) and treated cells.

The antibacterial activity of the PHBV/SiO_2 nanocomposites was tested against two test organisms viz. Gram-positive *Staphylococcus aureus* and Gram-negative *Escherichia coli*. All the samples were sterilised in an autoclave before the tests and then submerged in a 72 h old nutrient broth of $\sim 1.8 \times 10^6$ colony forming units per ml (CFU/mL). After incubation for 24 h at 37°C, the number of viable microorganism colonies was counted using a colony counter, and the results were stated as mean CFU/sample. The survival ratio (SR) was calculated using (5) [29]

$$\text{SR} = \frac{N}{N_o} \times 100 \tag{5}$$

where, N_o and N indicated the mean number of bacteria on the pure PHBV and the PHBV/SiO_2 nanocomposites, respectively. All the tests were carried out in triplicate, and the average values were reported.

2.6 Biodegradation study

Biodegradation study of PHBV and PHBV/SiO_2 nanocomposites films was carried out under environmental condition in the soil for a duration of 0th, 5th, 10th, 15th, 20th, 25th and 30th days. PHBV/SiO_2 nanocomposite film with 1.5 wt. % bSNPs content was used for the biodegradation study. Each sample with measurement of 5 × 5 cm film size was cut and buried into the soil which was collected from plastic dumping area and was sprinkled with water to maintain the moisture of the soil during the experimental period. Each set of experiments were conducted in triplicates. Each sample was dried and weighed gravimetrically before buried into the soil. Also, after the respective incubation periods, the samples were taken off cleaned, dried, and the weight loss was evaluated. The reduction in the weight of the degraded PHBV and PHBV/SiO_2 nanocomposite films buried in the soil after the degradation studies were determined using (6)

$$\text{Weight loss}(\%) = \frac{W_i - W_f}{W_i} \times 100 \tag{6}$$

where W_i is Initial Weight of the film and W_f is the Final Weight of the film

The degraded film strips were taken out after 0th, 15th and 30th days of incubation and washed with 2% sodium dodecyl sulphate to remove any soil debris and were vacuum-dried for overnight. The changes in the morphological and topological characteristics were analysed using SEM analysis [30].

2.7 Statistical analysis

All the experiments were conducted in triplicates ($n = 3$), and the results were presented in mean value with standard deviation (Mean ± SD). The experiments were followed by a completely randomised design (CRD) with three replicates for each treatment. All statistical analysis was performed with Graph Pad Prism software (version 5.03).

3 Results and discussion

3.1 Production and identification of extracted biopolymer

In this study, 3-hydroxybutyrate acid and 3-hydroxypentanoic acid were used as internal standards/positive control and the values of the peak areas were determined according to their retention time. According to the retention time, it can be preliminarily determined that the biopolymer accumulated by *W. anomalus* contained 3HB and 3HV, which indicated that PHBV was accumulated successfully by *W. anomalus* cells. The GC-MS chromatogram revealed significant peaks at retention time 2.57 and 8.17 min which were compared with the data from the mass spectrum library and were corresponding to that of methyl esters of 3-hydroxybutyrate (3HB) and 3-hydroxyvalerate 3HV respectively (see Fig. 1*a*). Characteristic molecular ion at m/z 103 and the major fragment ions at m/z 74, 54 and 43 were commonly observed for fragmentation pattern of methyl butenoates corresponded to methyl esters of 3-hydroxybutyrate. The molecular ion at m/z 113 and the specific fragment ions at m/z 87 and m/z 58 were commonly observed for fragmentation pattern of methyl pentenoates which are corresponding to methyl esters of 3-hydroxyvalerate [31]. Thus, it can be concluded that the biopolymer was PHA copolymer; moreover, it was composed of 3HB and 3HV monomers, and the species of PHA was PHBV. The ^{1}H NMR spectrum showed a signal at 0.93 and 1.26 ppm corresponding to the methyl group (-CH_3-) of hydroxy-valerate (HV) and hydroxybutyrate (HB), respectively (see Fig. 1*b*). The peak at 1.7 ppm corresponding to the methylene (-CH_2-) group of HV. The peaks at 2.45 and 2.56 ppm represented the methylene (-CH_2-) group of HV and HB, respectively. Signals at 5.27 ppm and 5.30–5.35 ppm corresponded to methine group (-CH-) of both HV and HB, respectively. The sharp peak at 7.76 ppm represented to that of $CDCl_3$. The ^{13}C NMR of the extracted biopolymer produced by *W. anomalus* VIT-NN01 showed signals at 70.2 ppm and 67.8–68.2 ppm corresponded to a methine group (CH) group of HV and HB, respectively. The peak at 37.7 and 40.7 ppm represented the methylene (CH_2) group of HV and HB, respectively. Another peak at 27.15 and 14.6 ppm represented the methylene (CH_2) group and CH_3 group of HV (see Fig. 1*b*). The prominent peak at 20.3 ppm corresponded the methyl (CH_3) group of HB. The peak at 169.7–169.9 ppm represented the ester (O-CH-) carbonyl (-C-) group of both HV and HB respectively. Thus, based on the GC-MS results, ^{1}H NMR and ^{13}C NMR spectrum, the extracted biopolymer was identified as Poly (3-hydroxybutyrate-*co*-3-hydroxyvalerate) (PHBV). A similar result was reported by Lee *et al.* [32] where palm kernel oil, crude palm oil, and palm olein produced PHBV using the bacteria *C. necator* DSM 545.

3.2 Surface morphology and elemental mapping

In this study, GS was used as precursor for synthesis of bSNPs. The sintered bSNPs showed a very bright white color and was found to be 33.3 g per 100 g of the incinerated GS ash. The TEM images of the bSNPs showed clusters of primary particles with a spherical shape and dimension of 50 nm diameter, as shown in Fig. 2*a*. A similar trend was reported by Athinarayanan *et al.* [19], where TEM images of bSNPs synthesized from rice husks showed clusters of primary particles with a spherical shape and a 10–30 nm diameter. The SEM micrograph revealed a cluster-like structure

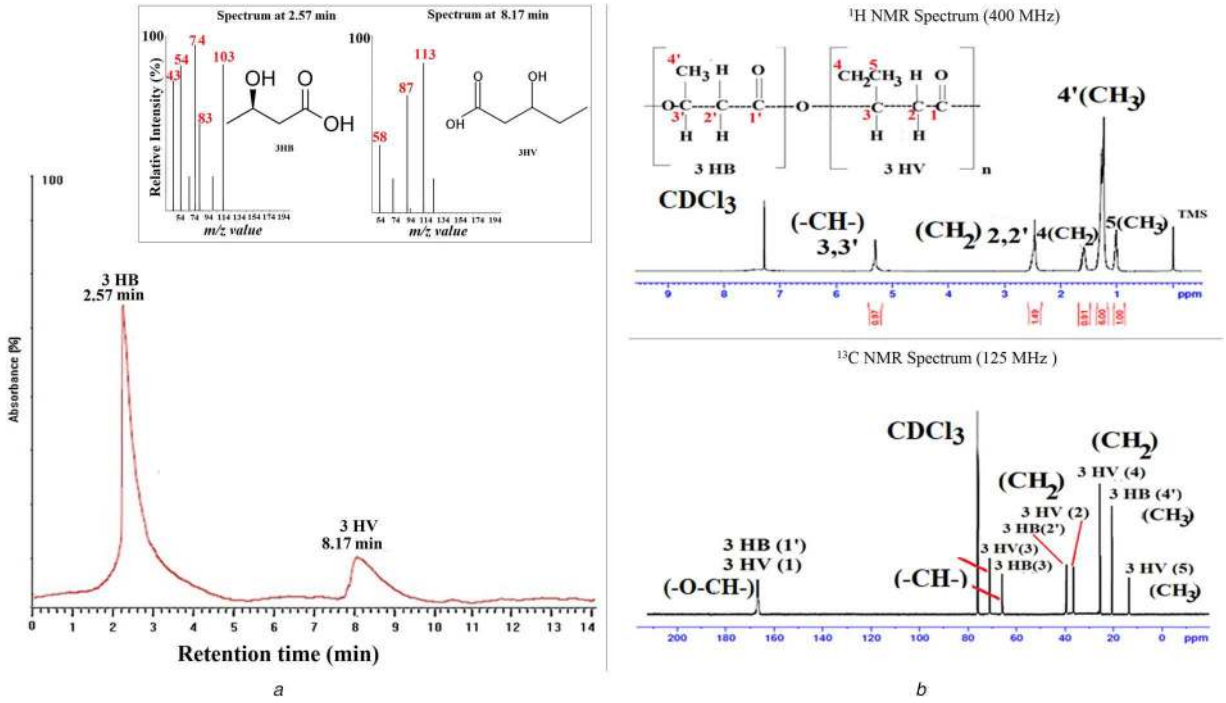

Fig. 1 *Identification of extracted biopolymer*
(a) GCMS analysis, ***(b)*** NMR analysis

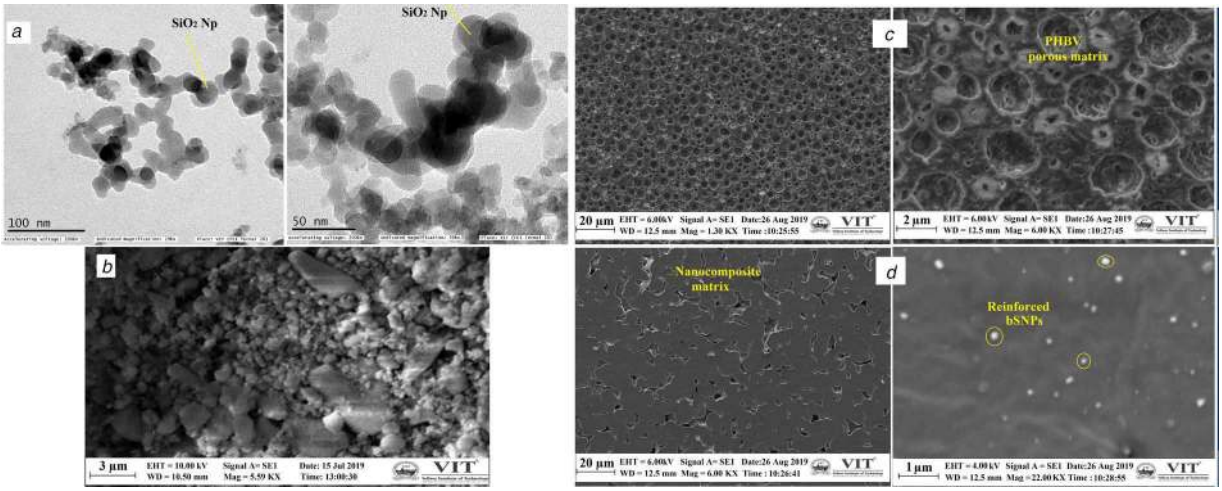

Fig. 2 *Morphological characterization*
(a) TEM micrographs of bSNPs, ***(b)*** SEM micrograph of bSNPs, ***(c)*** SEM micrographs of PHBV film, ***(d)*** SEM micrographs of PHBV/SiO_2 nanocomposite film

and agglomeration of bSNPs. The surface morphology of PHBV revealed a porous matrix of neat PHBV polymer with pore size around 700–900 nm as shown in Fig. 2*b*. However, in the micrographs of the fabricated PHBV/SiO_2 nanocomposite matrix exhibited spherical shaped and homogeneously dispersed silica-oxide nanoparticles (SiO_2NPs) onto the PHBV matrix (see Fig. 2*c*). The elemental composition of bSNPs revealed the presence of carbon (C), oxygen (O) and silica (Si) elements (see Fig. 3*a*). The carbon elements corresponded to the carbon-coated copper grids used to support the samples. Therefore, the EDX spectrum confirmed that the extracted sample was highly pure bSNPs and there is no other elemental impurities present in it except Si and O. The EDX spectrum of PHBV and PHBV/SiO_2 nanocomposite were shown in Figs. 3*b* and *c*, respectively. The EDX spectrum of the PHBV showed the presence of only C and O (See Fig. 3*b*). However, PHBV/SiO_2 revealed the presence of silica (Si) elements with along with C and O which confirmed the incorporation of SiO_2NPs within the PHBV matrix (see Fig. 3*c*).

3.3 FTIR analysis

The FTIR spectra of the bSNPs, PHBV and PHBV/SiO_2 nanocomposites reinforced with 0.5, 1.0, 1.5 and 2.0 wt % of bSNPs were shown in Fig. 4*a*. The bSNPs spectrum exhibited a vibration signal of Si-O-Si around 1072.42, 983.70, and 433.98–455.20 cm^{-1} assigned the asymmetric vibration, stretching vibration, and bending vibration of Si-O-Si, respectively [33]. The vibration at 1654.92 cm^{-1} corresponded to O-H bending. Additionally, broad peaks were observed around 3209.55–3047.5 cm^{-1} proved the presence of O-H stretching vibration due to the vibration of the silanol group on the silica surfaces. This finding was in agreement with the study reported by Adam *et al.* [34] on silica nanoparticles (SiNPs) [34]. The spectrum of PHBV exhibited a solid band at 1724.26 cm^{-1} arising from the C = O stretching of the ester group. The bands in the range of 1282.66–1020.34 cm^{-1} corresponded to C-O-C stretching vibrations, and the peaks at 2931.8 and 2883.58 cm^{-1} are related to C-H stretching bands. Further, the CH_3 asymmetric bending appeared at 1411.89 cm^{-1}, and the H-C-O in-plane bending is found at 1344.38 cm^{-1}. The

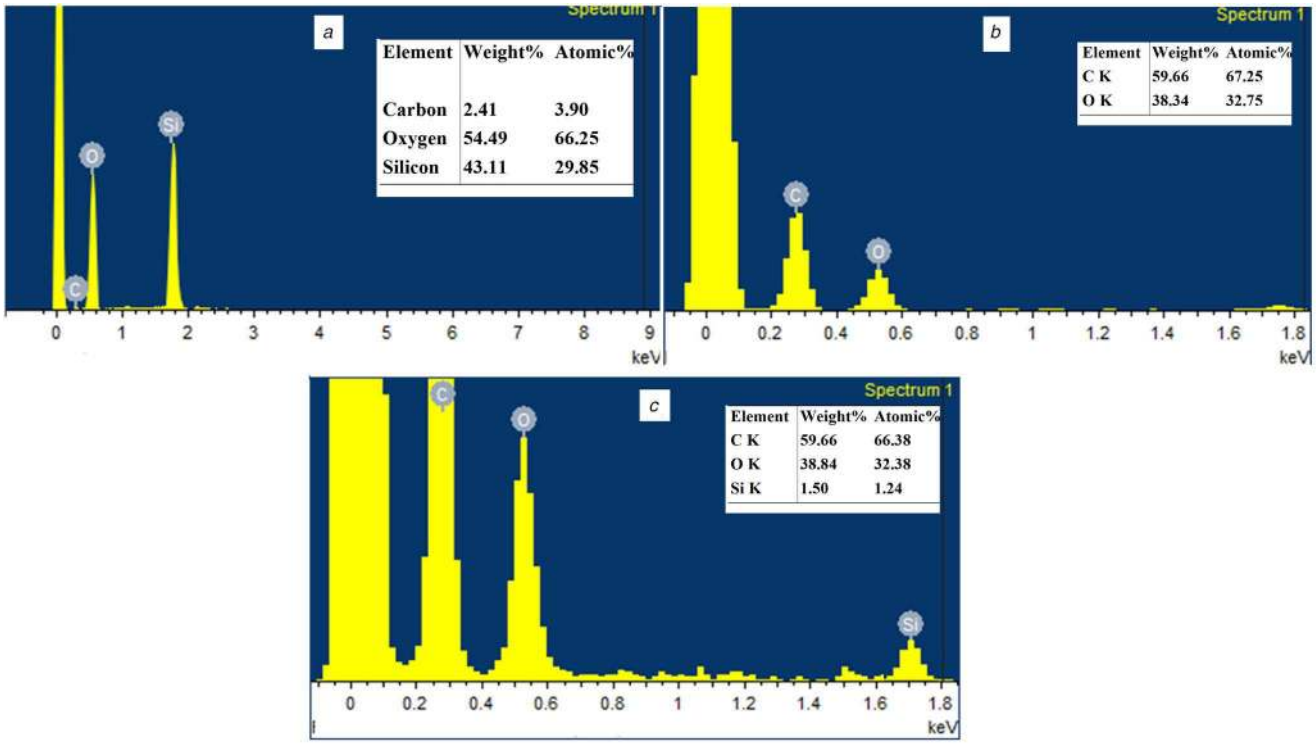

Fig. 3 *Elemental mapping*
(a) EDX of bSNPs, ***(b)*** EDX of PHBV film, ***(c)*** EDX of PHBV/SiO_2 nanocomposite film

spectra of the PHBV/SiO_2 nanocomposites showed the characteristic peaks of both PHBV and SiO_2. The sample with 0.5 to 2.0 wt % loading exhibited a broadening and upshifting of the peak corresponded to the hydroxyl stretching, exhibited at 3300 cm^{-1}. Such behaviour was attributed to the change from intramolecular to intermolecular hydroxyl-hydroxyl interactions [35] and suggested hydrogen bond formation with the carbonyl of the ester group of PHBV at the rate of breaking the hydrogen bonding among hydroxyl groups of the bSNPs. Moreover, the carbonyl band is broader, more intense and shifted to upper wavenumber, in comparison to that of the neat PHBV polymer which indicated the formation of hydrogen bonds with the hydroxyl moieties of the bSNPs. Further, the peaks assigned to the stretching of O-Si-O bonds appear at 1072.42 cm^{-1}, shifted to a lower wavelength near to 1000 cm^{-1} of the PHBV polymer (1020.34 cm^{-1}), is another indication of the strong SiO_2-matrix interactions. Hence, the shift and broadening of the bands related to the O-H and C = O stretching are considerably more pronounced, which indicated the increased nanofiller-matrix interactions upon rising bSNPs concentration.

3.4 XRD analysis

The X-ray diffraction patterns of the biogenic bSNPs, as shown in Fig. 4*b* revealed the presence of high purity amorphous silica. It can be seen that the highest broad scattering band was observed at 2θ value of about 22.57°, attributed to the amorphous structure and the broadness of the XRD peaks revealed that the synthesised biogenic silica was Nano scale in size. A similar report was observed by Carneiro *et al.* [36] at 2θ = 22.5° for nano-silica obtained from *Equisetum avenues*. The synthesis of amorphous bSNPs contributed to the positive impact in the formulation of PHBV nanocomposites because of its specific characteristics. The amorphous silica is more reactive and stable for a longer time as compared to the crystalline silica because of the presence of hydroxyl group in the amorphous region [37] noted in the present study which is more applicable to use in the reaction as compared to their crystalline region. The XRD diffractogram of PHBV revealed strong (0 0 4), (1 0 0), (0 1 5), (0 1 8), (1 1 4), (0 2 4) and (0 2 7) diffraction peaks at 2Θ = 28.37°, 32.27°, 43.97°, 57.33°, 63.27°, 73.02° and 83.73° which were corresponding to d spacing value of 3.2, 2.8, 2.0, 1.6, 1.2, and 1.1 Å respectively. The extracted PHBV retains a better crystallization property, and the increased intensity of peaks at 32.27° exhibited that the PHBV possibly a more structured arranged crystalline structure [38]. The average crystalline size of the PHA copolymer was calculated using the Scherer equation and found to be 158.64 A or 15.8 nm. The XRD diffractogram of PHBV nanocomposites blended with different concentration of SiO_2 NPs (0.5 to 2.0 wt %) were shown in Fig. 4*b*. A shift and broadening of the diffraction peak were observed in PHBV/SiO_2 nanocomposites as compared to the pure PHBV due to the presence of hydroxyl group present in the amorphous region of the bSNPs. This indicated the reorganization of the crystalline part into amorphous in the PHBV during blend and the presence of an intercalated nanostructure. The d_{121} spacing of Bragg angle 2Θ = 22.5° for SiO_2, PHBV/SiO_2 (2.0), PHBV/SiO_2 (1.5), PHBV/SiO_2 (1.0), and PHBV/SiO_2 (0.5), were 1.8, 2.8, 3.2, 3.9 and 4.05 nm, respectively. Interestingly, as the amount of SiO_2 present in nanocomposites decreases, the d-spacing systematically increases. By decreasing the nano-SiO_2 content in the nanocomposites, the amount of available space in the silicate layers decreases, which caused an increase in the d-spacing to accommodate the intercalated polymer chains. Similar behaviour was reported by Maiti *et al.* [39] where, synthetic fluoromica ion-exchanged with dimethyl ditallow ammonium (MAE) nanocomposites showed a gallery spacing increase from 2.9 to 3.5 nm in the nanocomposite.

3.5 Thermal properties

The thermal stability of the PHBV and PHBV/SiO_2 nanocomposites was analysed by TGA under a nitrogen atmosphere as shown in Fig. 5*a*. The TGA thermograms of PHBV and PHBV/SiO_2 nanocomposites were compared. An improvement in the thermal stability of the PHBV/SiO_2 was observed with the increasing concentration of bSNPs incorporated to PHBV matrix. The initial degradation temperature (*Ti*), and the rate of maximum degradation temperature (*Td*) of all the nanocomposites were tabulated in Table 1. The PHBV/SiO_2 nanocomposites and neat PHBV exhibited two step degradation stage (Table 1). In the first degradation step, thermogram showed a minor mass reduction due

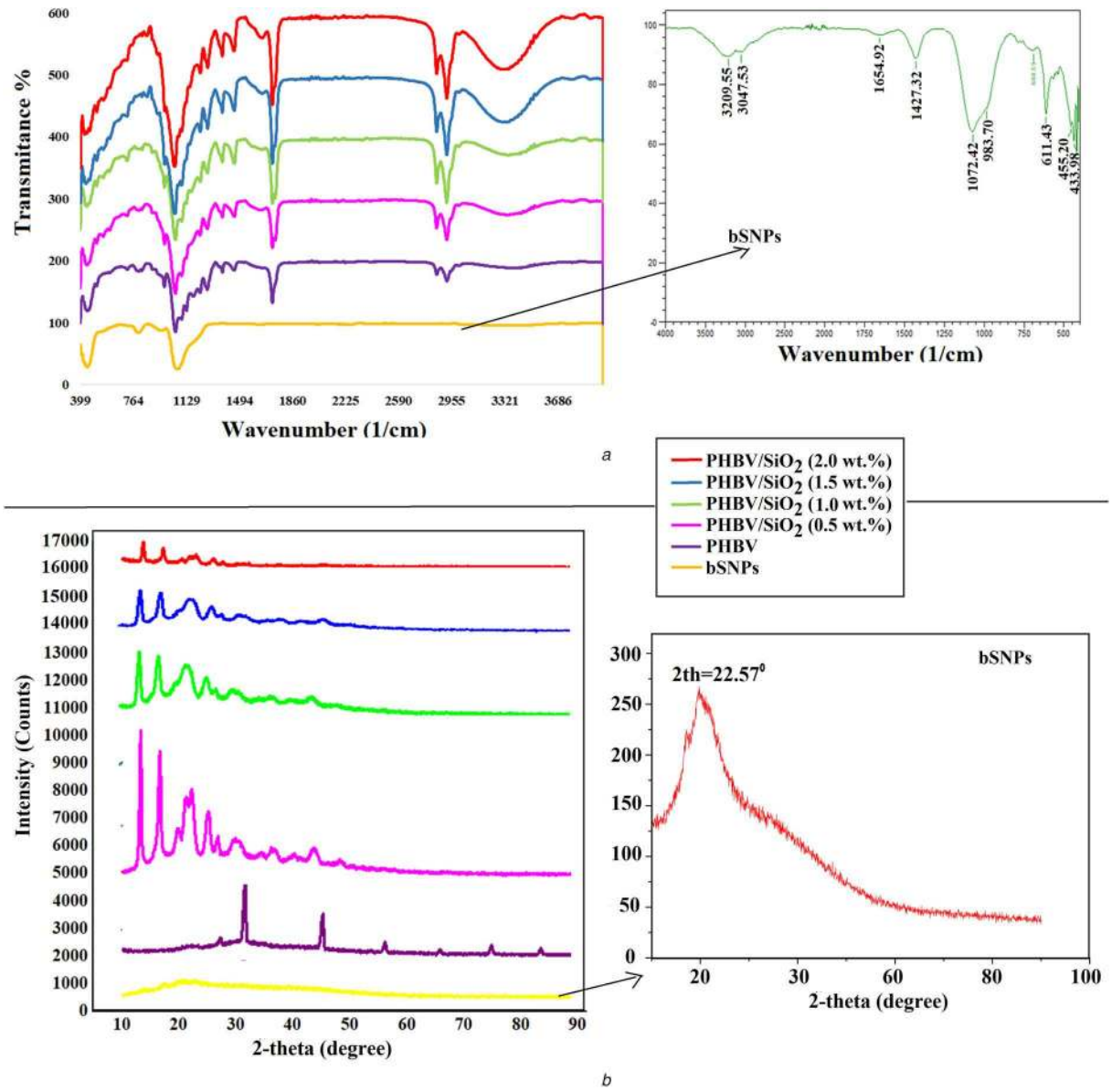

Fig. 4 *Physio-chemical characterization of bSNPs, PHBV and PHBV/SiO_2 nanocomposites*
(a) FTIR analysis, ***(b)*** XRD analysis

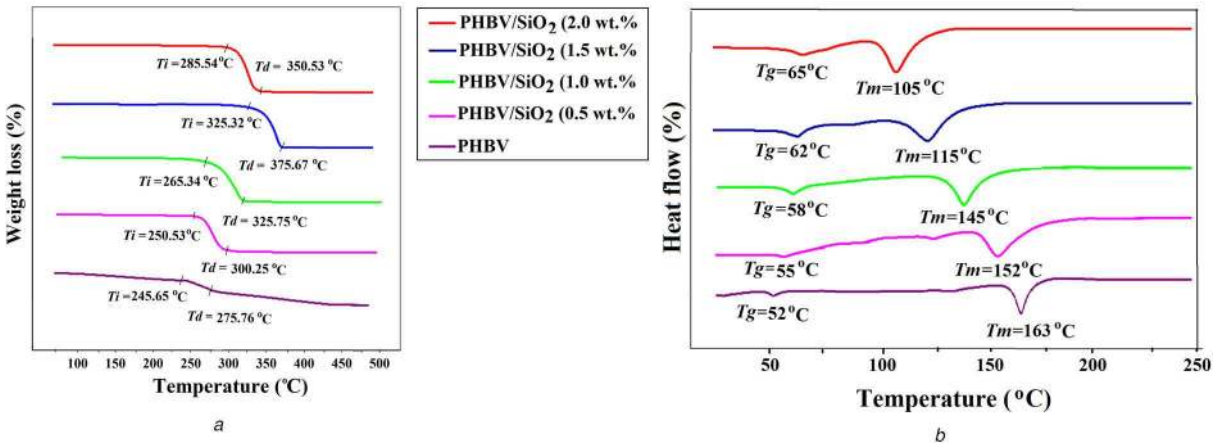

Fig. 5 *Thermal characterization of PHBV and PHBV/SiO_2 nanocomposites*
(a) TG analysis, ***(b)*** DSC analysis

to thermal degradation of the solvent such as water, lower molecular weight solvents present in the polymer or gas desorption taken place. In the second step, maximum mass loss of PHBV and PHBV/SiO_2 nanocomposites were observed from 245°C to 375.67°C due to degradation of low molecular weight compounds, ester cleavage of PHBV components and carbonization of hydrocarbonated compounds. The shifting of *Td* to higher temperatures, indicated that the thermal stabilisation effect was caused by the reinforced bSNPs. Moreover, a gradual increase in the char residue (Table 1) was observed with increasing bSNPs content, indicated

that the thermal decomposition of the matrix was retarded in the nanocomposites. The bSNPs act as insulator and bulk transport barriers that obstruct the escape of volatile products generated during the degradation process.Similar results were reported for Multi-walled carbon nanotubes (MWCNT) reinforced PHB nanocomposites [11], cellulose nanowhiskers (CNWs) [40] or silver sulphide (Ag_2S) nanoparticles [41].

DSC thermogram of PHBV and PHBV/SiO_2 nanocomposites were shown in Fig. 5*b*. PHBV exhibited an endotherm at 52°C corresponding to the glass transition temperature (*Tg*). All the PHBV/SiO_2 nanocomposites were found to have a higher *Tg* compared to the neat PHBV, as shown in Table 1. Also, with increasing of the bSNPs content, the *Tg* of PHBV/SiO_2 nanocomposites also increased. This indicated that reinforcement of bSNPs onto the polymer matrix prevented the segmental motion of polymer chains due to the hardness of bSNPs [42]. Another endotherm of neat PHBV was observed at high temperature (163°C), corresponding to the crystalline melting point (*Tm*) of PHBV. The *Tm* of PHBV/SiO_2 nanocomposites was found to be lower than that of the neat PHBV. In addition, the *Tm* of PHBV/SiO_2 nanocomposites was found to be decreased with increasing of the bSNPs concentration (Table 1). The results implied the crystalline of PHBV decreased because bSNPs added to PHBV matrix prevented the interaction of main chain and the formation of hydrogen bond [42]. Compared to PHBV, all the PHBV/SiO_2 nanocomposites showed a higher *Td*, which was far apart from its melting temperature *Tm*. This showed that PHBV/SiO_2 nanocomposites had better thermal stability and was not easy to be degraded in the process of processing. Also, the lower *Tm* implied the possibility of being processed at a lower temperature. Thus, the fabricated PHBV/SiO_2 nanocomposites have better prospect applications as compared to the PHBV.

3.6 Mechanical properties

The mechanical properties evaluated by tensile tests, and the values of Young's modulus (*E*), tensile strength (σ_y) and elongation at break (ε_b) were derived from the stress-strain curves of the different PHBV nanocomposites and shown in Fig. 6*a* and Table 1. The pure PHBV showed Young's modulus of ∼1.08 GPa. The addition of bSNPs leads to a gradual rise in *E* (see Fig. 6*a*). The mechanical properties of polymer nanocomposites are affected mostly by the filler-matrix interactions, state of dispersion of nanofiller and degree of crystallinity of the matrix. Thus, the substantial *E* enhancement attained in the fabricated PHBV/SiO_2 nanocomposites was attributed to a robust interfacial adherence between the phases through interactions via H-bonding, good bSNPs dispersion, and the increase in the crystallinity of PHBV. However, at higher content of bSNPs the *E*, σ_y and ε_b dropped moderately. It can be concluded that nanocomposites with higher loadings of the bSNPs restrict the ductile flow of the polymer chains, which was reflected in lower ε_b values. These results indicated that the incorporation of small amounts of bSNPs improves the ability of PHBV to absorb energy during the deformation process [43]. The impact strength measurements of PHBV and PHBV/SiO_2 nanocomposites were plotted in Fig. 6*a*. The incorporation of 1.5 wt% bSNPs leads to a significant improvement in the impact resistance of the PHBV as compared to the lowest (0.5 wt %) and highest (2.0 wt %) content of bSNPs. It was reported that the shape, size, state of dispersion of the filler and its interfacial adhesion with the matrix have a strong influence on the rate of energy absorption, hence on the impact properties of PHBV nanocomposites [44]. The impact strength of PHBV nanocomposite (2.0 wt %), showed the presence of small bSNPs clusters which might nucleate a few cracks or promote the formation of little dimples, leading to a slight reduction in ductility. Therefore, PHBV/SiO_2 nanocomposites loaded with 0.5–1.5 wt % bSNPs were found to be useful for enhancing the impact strength of PHBV.

The water uptake capacity of the PHBV/SiO_2 nanocomposites was shown in Fig. 6*b*. The strength of interaction between water molecules and an oxidized silicon nanoparticle surface is higher than that with a pure silicon surface. The result indicated that water uptake capability of the nanocomposites decreases with increasing SiO_2 content, by up to 91.8% at 1.5 wt % nanoparticle content, which indicated the improved barrier property against water for the nanocomposites in comparison to the pure PHBV. The above findings suggested that reinforcement of bSNPs into PHBV was an effective way to obtain strong and improved intercalated organic-inorganic hybrids as observed in XRD diffractogram. On increasing the concentration of bSNPs, the reactive hydroxy group present at the surface also increases and impregnated easily with the PHBV matrix. And formed an intermolecular hydroxyl-hydroxyl interactions between the surface hydroxyl moieties of the bSNPs (–OH- bond of the silanol) and the carbonyl of the ester group of PHBV as observed in FTIR spectrum. This copolymerization resulted in the increase in the hydrophobicity and barrier properties of the PHBV/SiO_2 nanocomposites [42].

3.7 Biocompatibility and antibacterial properties

The in vitro biocompatibility of the nanocomposites was evaluated using the MTT assay, and the results were shown in Fig. 6*c*. The fibroblast L929 cells were exposed to the sterile discs of fabricated PHBV/SiO_2 nanocomposite films impregnated with 0.0, 0.5, 1.0, 1.5 and 2.0 wt % of bSNPs for 24, 48 and 72 h. The results revealed that the PHBV/SiO_2 nanocomposites showed 98% cell viability which indicated that the reinforced bSNPs had no toxicity towards the treated cells. The findings showed no significant changes in cell viability when bSNPs were incorporated to the PHBV polymer at a concentration of up to 2.0 wt %. Thus, it can be concluded that the fabricated PHBV/SiO_2 nanocomposites were non-toxic and biocompatible and hence, this biomaterial can be used as biomedical or food packaging biomaterials [45].

The antibacterial action of the pure extracted PHBV and PHBV/SiO_2 nanocomposites were tested against two human pathogenic bacteria: *E. coli* (Gram-negative) and *S. aureus* (Gram-positive), and the results were shown in Fig. 6*c*. After 24 h of the incubation period, the viable bacterial colonies were counted in CFU/sample, and the survival ratio (%) was calculated (see Fig. 6*c*). The results showed that the survival ratio of *E. coli* and *S. aureus* decreases exponentially with increasing bSNPs content. A similar report was demonstrated by Mukheem *et al.* [46], where PHA/Graphene Silver nanocomposite showed reduction of *S. aureus* and *E. coli* as compared to bare PHA in 2 h of time. In the present study, the maximum antibacterial activity (about 94.7 and 92% growth inhibition for *E. coli* and *S. aureus*, respectively) was attained with 2.0 wt % loading which could be because of the larger size of bSNPs providing active surface area reactivity. Interestingly, the antibacterial effect of PHBV nanocomposites on *E. coli* was systematically stronger than on *S. aureus* due to the structural and chemical compositional differences of the Gram-

Table 1 Mechanical and thermal parameters

Samples	*Tg*, °C	*Tm*, °C	*Ti*, °C	*Td*, °C	Char residue, %	ε_b, %	*E*, GPa	σy, MPa
PHBV	52	163	245.65	275.76	1.2	44.00	1.08	1.48
PHBV/SiO_2 (0.5 wt. %)	55	152	250.53	300.25	5.8	43.40	1.33	3.00
PHBV/SiO_2 (1.0 wt. %)	58	145	265.34	325.75	11.3	42.40	1.90	4.30
PHBV/SiO_2 (1.5 wt. %)	62	115	325.32	375.67	13.9	5.040	3.42	18.13
PHBV/SiO_2 (2.0 wt. %)	65	105	285.54	350.53	15.6	2.859	2.58	8.20

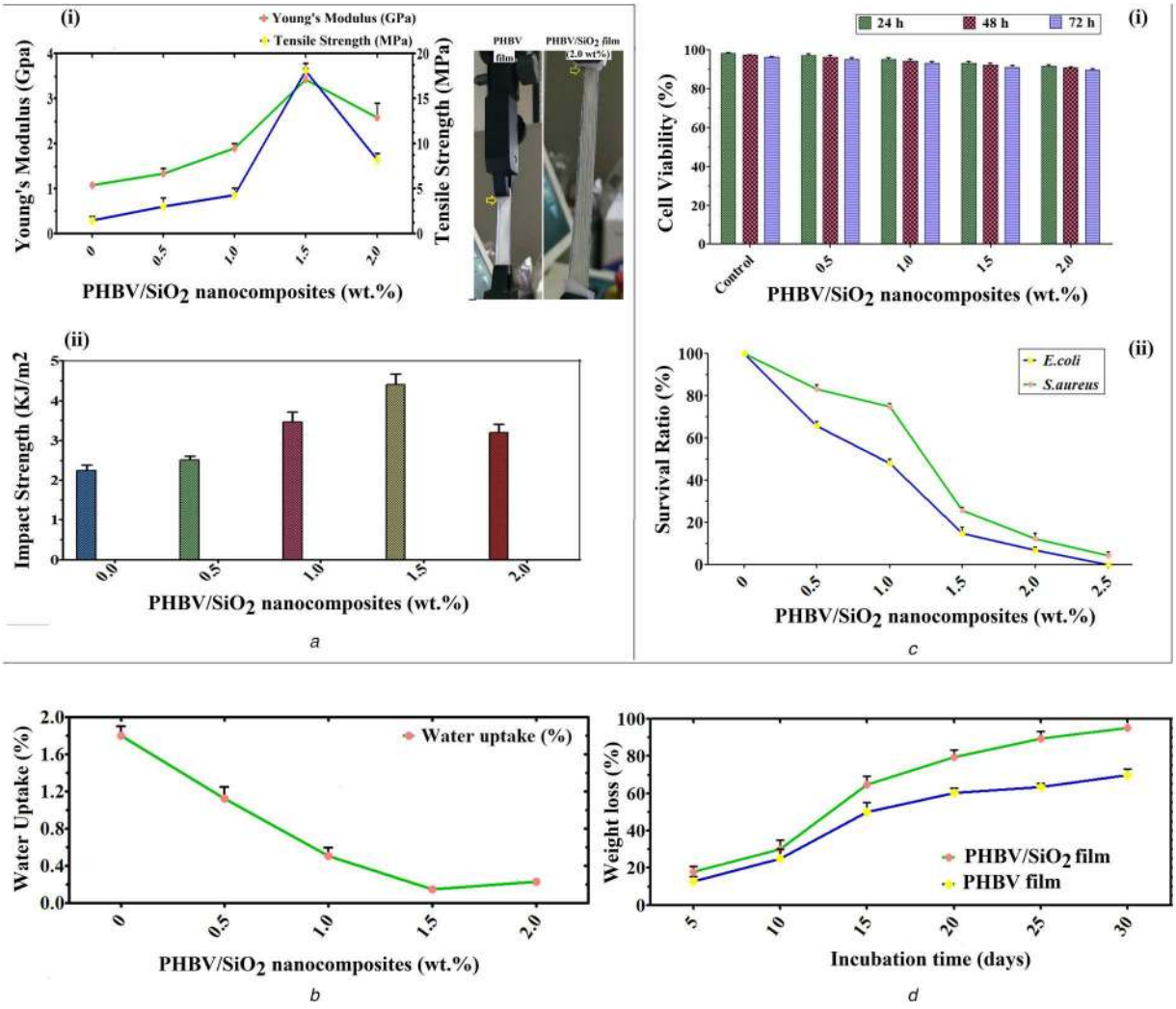

Fig. 6 *Improved properties of PHBV/SiO_2 nanocomposites*

(a) Mechanical properties PHBV and PHBV/SiO_2 nanocomposites by Young's Modulus and Tensile Strength (i), Impact Strength (ii), ***(b)*** Water uptake capacity test, ***(c)*** Biocompatibility and Antibacterial properties by Cell viability assay (i), Antibacterial assay (ii), ***(d)*** Weight loss percentage of degraded PHBV and PHBV/SiO_2 nanocomposite film

positive (one cytoplasmic membrane and a thick wall of multilayer peptidoglycan) and Gram-negative (more complex cell wall structure, with a layer of peptidoglycan between the outer and the cytoplasmic membrane) bacterial cell walls [47]. The mechanism of action of bSNPs against both the bacteria was attributed to the severe damage in their outer membrane and loss of their cellular reliability while contacting with bSNPs. Also, the water-repelling properties and positively charged bSNPs may have interacted with the lipid bilayer structures of the bacterial membranes, which led to the eradication and death of cells [48]. Therefore, the results demonstrated the enormous potential of the fabricated PHBV/SiO_2 nanocomposites with antimicrobial activity to prevent the growth of pathogenic and spoilage microorganisms. These nanocomposites could be served as effective food packaging biomaterial.

3.8 Biodegradation study

The reduction in the weight of the degraded films was evaluated after 30 days of incubation. The weight of PHBV film was reduced from 0.2589 to 0.129 and 0.077 g after 15th and 30th days of incubation respectively. Similarly, the weight of PHBV/SiO_2 films reduced from 0.2787 to 0.098 (64.66%) and 0.013 g (95.3%) after 15th and 30th days of incubation period respectively. The percentage of the total weight loss of the PHBV/SiO_2 films after 15th and 30th days of incubation were found to be 64.66 and 95.3% which was quite higher as compared to the PHBV films (50 and 70%) respectively as shown in Fig. 6*d*. The surface morphological and topological study of the degraded films were observed by SEM analysis. No apparent structural changes were found on the 0th day of the PHBV and PHBV/SiO_2 nanocomposites which were used as control (see Fig. 7*a*). However, attachment of fungal spores and mycelium network formation was observed after 15th days of incubation period on the surface of both the films, as shown in Fig. 7*b*. In the case of PHBV films, spores attachment and mycelium network formation with very few structural changes were observed after 30 days of degradation (see Fig. 7*c*). However, in case of PHBV/SiO_2 nanocomposites films, significant structural changes like grooves, cracks, pits, damaged layer and roughening of the surface were observed after 30th days of degradation as shown in Fig. 7*c*. Thus, the presence of grooves and cracks confirmed the fragility brought about to the PHBV/SiO_2 nanocomposite films due to the potential plastic degrading microorganisms present in the soil. The colonization, bio-film, and mycelium network formation on the nanocomposite sheets showed that the microorganisms utilized PHBV as the sole source of carbon. Significant biodegradation with most of the spherulitic aggregate morphology destroyed by the microorganisms was observed in PHBV/SiO_2 nanocomposite. In contrast, PHBV films exhibited less degradation keeping the spherulitic morphology almost intact. The faster biodegradation in the nanocomposites was due to the smaller spherulites, which in turn result in higher amounts of inter spherulitic area, which are prone to hydrolysis followed by consumption by the microorganisms [19]. Although the biodegradation of neat PHB enzymatically [49] and in seawater [50] has already been studied, this is the first report of biodegradability of PHBV/SiO_2 nanocomposites which showed 95.3% degradation on 30th day under natural condition.

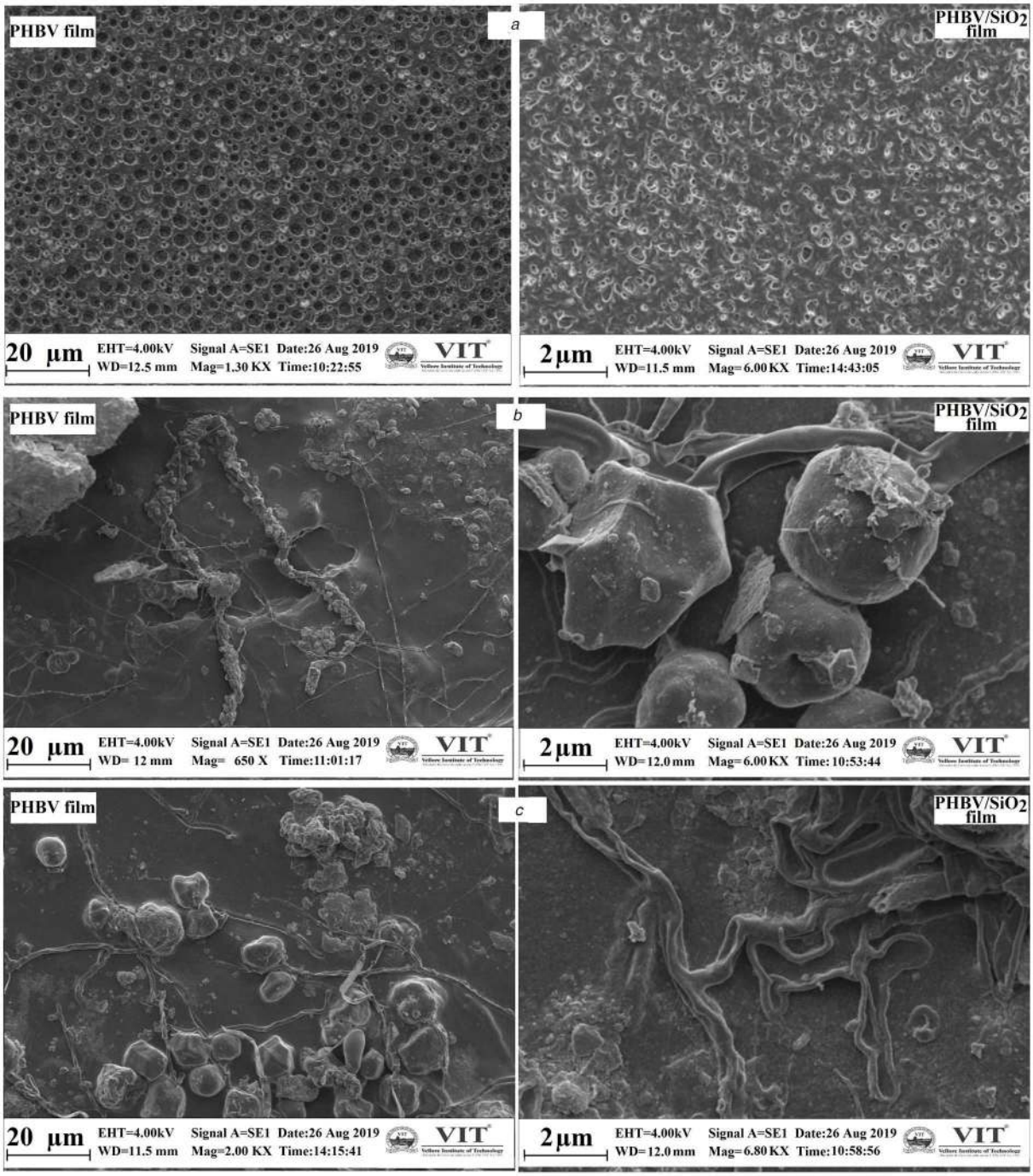

Fig. 7 *Surface topology of degraded PHBV and PHBV/SiO_2 nanocomposite films by SEM analysis*
(a) 0th day, ***(b)*** 15th days, ***(c)*** 30th days

3.9 Statistical analysis

The findings of water uptake capacity, biocompatibility test and antibacterial activity were analysed by two-way ANOVA that showed p-value is less than 0.0001, which indicated that the interaction is extremely significant, as shown in Table 2.

4 Conclusions

The bSNPs were synthesised using GS as a precursor, and the novel PHBV/SiO_2 biodegradable nanocomposites were fabricated via simple solution casting method to improve its physical, chemical, thermal, mechanical, barrier, biodegradable, biocompatible, and antibacterial properties. The FTIR spectra demonstrated the existence of strong hydrogen bonding interactions between the surface hydroxyl moieties of the bSNPs and the carbonyl of the ester groups of PHBV. The PHBV/SiO_2 nanocomposites showed significant improvement in the thermal, mechanical, heat resistance and barrier properties of the pure PHBV matrix on the addition of bSNPs which was due to the homogenous bSNPs dispersion and its strong interfacial adhesion with the matrix through hydrogen bonding interactions. The PHBV/SiO_2 nanocomposites revealed excellent biocompatible, biodegradable and antimicrobial properties which could be highly useful to minimise the growth of contaminant microorganisms, extending the shelf-life of food and improving its quality. Therefore, the fabricated PHBV/SiO_2 nanocomposites can serve as an eco-friendly, cost-effective alternative to the synthetic plastic food packaging materials.

5 Acknowledgments

This study was funded by Council of Scientific and Industrial Research (CSIR), India, grant (09/844(0071)/2019-EMR-I), New Delhi, India. Authors are thankful to School of Advanced Sciences

Table 2 ANOVA results

SV[a]	Df[b]				Mean square				Sum of square				*F* value				*P* value			
Tests	σy	W[c]	B[d]	A[e]	σy	W[c]	B[d]	A[e]	σy	W[c]	B[d]	A[e]	σy	W[c]	B[d]	A[e]	σy	W[c]	B[d]	A[e]
I[f]	4	5	8	5	50	647	5	143	200	129	12	718	156	9.6	1	46		<0.0001*		
CF[g]	1	1	2	1	184	2271	15	1056	184	2271	30	1056	575	169	22	339		<0.0001*		
RF[h]	4	5	4	5	86	22,650	67	9435	347	4530	269	47,180	270	337	101	303		<0.0001*		

*Significant.

[a]Source of variance.

[b]Degree of freedom.

[c]Water uptake.

[d]Biocompatibility test.

[e]Antibacterial activity.

[f]Interaction.

[g]Column factor.

[h]Row factor.

(SAS), School of Bio-Medical Sciences (SBST) and DST-FIST/VIT SEM of Vellore Institute of Technology, India for providing laboratory facilities while conducting the experimental work.

6 References

[1] Marsh, K., Bugusu, B.: 'Food packaging -roles, materials, and environmental issues', *J. Food Sci.*, 2007, **72**, (3), pp. 39–55

[2] Moreno, M.A., Orqueda, M.E., Gómez-Mascaraque, L.G., *et al.*: 'Crosslinked electrospun zein-based food packaging coatings containing bioactive chilto fruit extracts', *Food Hydrocoll.*, 2019, **95**, pp. 496–505

[3] Bordes, P., Pollet, E., Avérous, L.: 'Nano-biocomposites: biodegradable polyester/nanoclay systems', *Prog. Polym. Sci.*, 2009, **34**, (2), pp. 125–155

[4] Rhim, J.W., Park, H.M., Ha, C.S.: 'Bio-nanocomposites for food packaging applications', *Prog. Polym. Sci.*, 2013, **38**, (10–11), pp. 1629–1652

[5] Pérez-Arauz, A.O., Aguilar-Rabiela, A.E., Vargas-Torres, A., *et al.*: 'Production and characterization of biodegradable films of a novel polyhydroxyalkanoate (PHA) synthesized from peanut oil', *Food Packag. Shelf Life*, 2019, **20**, p. 100297

[6] Bhatia, S.K., Wadhwa, P., Hong, J.W., *et al.*: 'Lipase mediated functionalization of poly (3-hydroxybutyrate-co-3-hydroxyvalerate) with ascorbic acid into an antioxidant active biomaterial', *Int. J. Biol. Macromol.*, 2019, **123**, pp. 117–123

[7] Jeon, J.M., Kim, H.J., Bhatia, S.K., *et al.*: 'Application of acetyl-CoA acetyl transferase (AtoAD) in Escherichia coli to increase 3-hydroxyvalerate fraction in poly (3-hydroxybutyrate-co-3-hydroxyvalerate)', *Bioprocess Biosyst. Eng.*, 2017, **40**, pp. 781–789

[8] Jaiswal, L., Shankar, S., Rhim, J.W.: 'Applications of nanotechnology in food microbiology', *Methods Microbiol.*, 2019, **46**, pp. 43–60

[9] Schmatz, D.A., Costa, J.A.V., de Morais, M.G.: 'A novel nanocomposite for food packaging developed by electrospinning and electrospraying', *Food Packag. Shelf Life*, 2019, **20**, p. 100314

[10] Goudarzi, V., Shahabi-Ghahfarrokhi, I.: 'Development of photo-modified starch/kefiran/TiO_2 bio-nanocomposite as an environmentally-friendly food packaging material', *Int. J. Biol. Macromol.*, 2018, **116**, pp. 1082–1088

[11] Xu, C., Qiu, Z.: 'Crystallization behavior and thermal property of biodegradable poly(3-hydroxybutyrate)/multi-walled carbon nanotubes nanocomposite', *Polym. Adv. Technol.*, 2011, **22**, (5), pp. 538–544

[12] Prakalathan, K., Mohanty, S., Nayak, S.K.: 'Reinforcing effect and isothermal crystallization kinetics of poly(3-hydroxybutyrate) nanocomposites blended with organically modified montmorillonite', *Polym. Compos.*, 2014, **35**, (5), pp. 999–1012

[13] Sudesh, K., Abe, H., Doi, Y.: 'Synthesis, structure and properties of polyhydroxyalkanoates: biological polyesters', *Prog. Polym. Sci.*, 2000, **25**, (10), pp. 1503–1555

[14] Vogel, C., Wessel, E., Siester, H.W.: 'FT-IR imaging spectroscopy of phase separation in blends of poly(3-hydroxybutyrate) with poly(L-lactic acid) and poly(ε-caprolactone)', *Biomacromolecules*, 2008, **9**, (2), pp. 523–527

[15] Maiti, P., Batt, C.A., Giannelis, P.: 'New biodegradable polyhydroxybutyrate/layered silicate nanocomposites', *Biomacromolecules*, 2007, **8**, (11), pp. 3393–3400

[16] Basumatary, K., Daimary, P., Das, S.K., *et al.*: 'Lagerstroemia speciosa fruit-mediated synthesis of silver nanoparticles and its application as filler in agar based nanocomposite films for antimicrobial food packaging', *Food Packag. Shelf Life*, 2018, **17**, pp. 99–106

[17] Ojha, N., Das, N.: 'A statistical approach to optimize the production of polyhydroxyalkanoates from Wickerhamomyces anomalus VIT-NN01 using response surface methodology', *Int. J. Biol. Macromol.*, 2018, **107**, pp. 2157–2170

[18] Huang, P., Okoshi, T., Mizuno, S., *et al.*: 'Gas chromatography-mass spectrometry-based monomer composition analysis of medium-chain-length polyhydroxyalkanoates biosynthesized by Pseudomonas spp', *Biosci. Biotechnol. Biochem.*, 2018, **82**, pp. 1615–1623

[19] Athinarayanan, J., Periasamy, V.S., Alhazmi, M., *et al.*: 'Synthesis of biogenic silica nanoparticles from rice husks for biomedical applications', *Ceram. Int.*, 2015, **41**, (1), pp. 275–281

[20] Naddaf, M., Kafa, H., Ghanem, I.: 'Extraction and characterization of nano-silica from olive stones', *Silicon*, 2020, **12**, pp. 185–192

[21] Herrera, N.N., Letoffe, J.M., Reymond, J.P., *et al.*: 'Silylation of laponite clay particles with mono functional and trifunctional vinyl alkoxysilanes', *J. Mater. Chem.*, 2005, **15**, (8), pp. 863–871

[22] Phukon, P., Saikia, J.P., Konwar, B.K.: 'Bio-plastic (P-3HB-co-3HV) from Bacillus circulans (MTCC 8167) and its biodegradation', *Colloids Surf. B*, 2012, **92**, pp. 30–34

[23] Salgaonkar, B.B., Braganc, J.M.: 'Biosynthesis of poly(3-hydroxybutyrate-co-3-hydroxyvalerate) by Halogeometricum borinquensestrain E3', *Int. J. Biol. Macromol.*, 2015, **78**, pp. 339–346

[24] Dhangdhariya, J.H., Dubey, S., Trivedi, H.B., *et al.*: 'Polyhydroxyalkanoate from marine Bacillus megaterium using CSMCRI's dry sea mix as a novel growth medium', *Int. J. Biol. Macromol.*, 2015, **76**, pp. 254–261

[25] ASTM D638-14: '*Standard test method for tensile properties of plastics*', 2014, DOI: 10.1520/D0638-14

[26] ASTM D6110-10: '*Standard test method for determining the Charpy impact resistance of notched specimens of plastics*', 2010, DOI: 10.1520/D6110-10

[27] Díez-Pascual, A., Díez-Vicente, A.: 'Poly (3-hydroxybutyrate)/ZnO bionanocomposites with improved mechanical, barrier and antibacterial properties', *Int. J. Mol. Sci.*, 2014, **15**, (6), pp. 10950–10973

[28] Tang, S., Tian, B., Guo, Y.J., *et al.*: 'Chitosan/carbonated hydroxyapatite composite coatings: fabrication, structure and biocompatibility', *Surf. Coat. Technol.*, 2014, **251**, pp. 210–216

[29] Kanmani, P., Rhim, J.W.: 'Properties and characterization of bionanocomposite films prepared with various biopolymers and ZnO nanoparticles', *Carbohydr. Polym.*, 2014, **106**, pp. 190–199

[30] Ojha, N., Pradhan, N., Singh, S., *et al.*: 'Evaluation of HDPE and LDPE degradation by fungus, implemented by statistical optimization', *Sci. Rep.*, 2017, **7**, (1), pp. 1–13

[31] Sato, H., Hoshino, M., Aoi, H., *et al.*: 'Compositional analysis of poly (3-hydroxybutyrate-co-3-hydroxyvalerate) by pyrolysis-gas chromatography in the presence of organic alkali', *J. Anal. Appl. Pyrolysis.*, 2005, **74**, pp. 193–199

[32] Lee, W.H., Loo, C.Y., Nomura, C.T., *et al.*: 'Biosynthesis of polyhydroxyalkanoate copolymers from mixtures of plant oils and 3-hydroxyvalerate precursors', *Bioresour. Technol.*, 2008, **99**, (15), pp. 6844–6851

[33] Gu, S., Zhou, J., Luo, Z., *et al.*: 'A detailed study of the effects of pyrolysis temperature and feedstock particle size on the preparation of nanosilica from rice husk', *Ind. Crops. Prod.*, 2013, **50**, pp. 540–549

[34] Adam, F., Chew, T.S., Andas, J.: 'A simple template-free sol–gel synthesis of spherical nanosilica from agricultural biomass', *J. Sol-Gel Sci. Technol.*, 2011, **59**, (3), pp. 580–583

[35] Zuza, E., Lejardi, A., Ugartemendia, J.M., *et al.*: 'Compatibilization through specific interactions and dynamic fragility in poly (D, L-lactide)/polystyrene blends', *Macromol. Chem. Phys.*, 2008, **209**, (23), pp. 2423–2433

[36] Carneiro, M.E., Magalhães, W.L., Bolzon de Muñiz, G.I., *et al.*: 'Preparation and characterization of nano silica from Equisetum arvenses', *Embrapa Florestas-Artigo em Periódico Indexado (ALICE)*, 2015, **5**, (2), p. 7

[37] Varshney, V.K., Naithani, S.: 'Chemical functionalization of cellulose derived from nonconventional sources', in Kalia, S., Kaith, B., Kaur, I. (Eds.): '*Cellulose fibers: bio-and nano-polymer composites*' (Springer, Berlin, Heidelberg, 2011), pp. 43–60

[38] Reddy, S.V., Thirumala, M., Mahmood, S.K.: 'Production of PHB and P(3HB-co-3HV) biopolymers by Bacillus megaterium strain OU303A isolated from municipal sewage sludge', *World J. Microbiol. Biotechnol.*, 2009, **25**, pp. 391–397

[39] Maiti, P., Nam, P.H., Okamoto, M., *et al.*: 'Influence of crystallization on intercalation, morphology, and mechanical properties of polypropylene/clay nanocomposites', *Macromolecules*, 2002, **35**, (6), pp. 2042–2049

[40] Yeo, S.Y., Tan, W.L., Bakar, M.A., *et al.*: 'Silver sulfide/poly(3-hydroxybutyrate) nanocomposites: thermal stability and kinetic analysis of thermal degradation', *Polym. Degrad. Stab.*, 2010, **95**, (8), pp. 1299–1304

[41] de Oliveira Patricio, P.S., Pereira, F.V., dos Santos, M.C., *et al.*: 'Increasing the elongation at break of polyhydroxybutyrate biopolymer: effect of cellulose nanowhiskers on mechanical and thermal properties', *J. Appl. Polym. Sci.*, 2013, **127**, (5), pp. 3613–3621
[42] Jia, X., Li, Y., Cheng, Q., *et al.*: 'Preparation and properties of poly (vinyl alcohol)/silica nanocomposites derived from copolymerization of vinyl silica nanoparticles and vinyl acetate', *Eur. Polym. J.*, 2007, **43**, pp. 1123–1131
[43] Thomas, S., Zaikov, G.E.: '*Polymer nanocomposites research advances*' (Nova Science Publishers, Inc., New York, NY, USA, 2008), p. 9
[44] Sanchez-Garcia, M.D., Lagaron, J.M., Hoa, S.V.: 'Effect of addition of carbon nanofibers and carbon nanotubes on properties of thermoplastic biopolymers', *Compos. Sci. Technol.*, 2010, **70**, (7), pp. 1095–1105
[45] Ute, S., Schroder, H.C., Wang, X., *et al.*: 'Alginate/silica composite hydrogel as a potential morphogenetically active scaffold for three-dimensional tissue engineering', *RSC Adv.*, 2013, **3**, (28), pp. 11185–11194
[46] Mukheem, A., Muthoosamy, K., Manickam, S., *et al.*: 'Fabrication and characterization of an electrospun pha/graphene silver nanocomposite scaffold for antibacterial applications', *Materials*, 2018, **11**, p. 1673
[47] Song, J., Kong, H., Jang, J.: 'Bacterial adhesion inhibition of the quaternary ammonium functionalized silica nanoparticles', *Colloids Surf. B*, 2011, **82**, (2), pp. 651–656
[48] Chitra, K., Annadurai, G.: 'Fluorescent silica nanoparticles in the detection and control of the growth of pathogen', *J. Nanotechnol.*, 2013, **2013**, pp. 1–7
[49] Scandola, M., Focarete, M.L., Frisoni, G.: 'Simple kinetic model for the heterogeneous enzymatic hydrolysis of natural poly (3-hydroxybutyrate)', *Macromolecules*, 1998, **31**, (12), pp. 3846–3851
[50] Tsuji, H., Suzuyoshi, K.: 'Environmental degradation of biodegradable polyesters 1. Poly (ε-caprolactone), poly [(R)-3-hydroxybutyrate], and poly (L-lactide) films in controlled static seawater', *Polym. Degrad. Stab.*, 2002, **75**, (2), pp. 347–355